ISPRS Journal of Photogrammetry and Remote Sensing 89 (2014) 49–58

Contents lists available at ScienceDirect

ISPRS Journal of Photogrammetry and Remote Sensing

journal homepage: www.elsevier.com/locate/isprsjprs

Above ground biomass estimation in an African tropical forest with lidar and hyperspectral data

Gaia Vaglio Laurin [a,f,*], Qi Chen [b], Jeremy A. Lindsell [c], David A. Coomes [d], Fabio Del Frate [f], Leila Guerriero [f], Francesco Pirotti [g], Riccardo Valentini [e,a]

[a] CMCC – Centro Mediterraneo per i Cambiamenti Climatici, (Euro-Mediterranean Center for Climate Change), IAFENT Division, via Pacinotti 5, Viterbo 01100, Italy
[b] Department of Geography, University of Hawai'i at Mānoa, 422 Saunders Hall, 2424 Maile Way, Honolulu, HI 96822, USA
[c] The Royal Society for the Protection of Birds, The Lodge, Sandy, Beds. SG19 2DL, UK
[d] Forest Ecology and Conservation Group, Department of Plant Sciences, University of Cambridge, Downing Street, Cambridge CB2 3EA, UK
[e] Department of Forest Resources and Environment, University of Tuscia, Viterbo 01100, Italy
[f] Tor Vergata University, Department of Civil Engineering and Computer Sciences, Via del Politecnico 1, Rome 00133, Italy
[g] CIRGEO – Interdepartmental Research Center of Geomatics, University of Padova, Via dell'Università 16, Legnaro 35020, Italy

ARTICLE INFO

Article history:
Received 30 May 2013
Received in revised form 21 November 2013
Accepted 7 January 2014
Available online 31 January 2014

Keywords:
Lidar
Hyperspectral
Forestry
Africa
Biomass

ABSTRACT

The estimation of above ground biomass in forests is critical for carbon cycle modeling and climate change mitigation programs. Small footprint lidar provides accurate biomass estimates, but its application in tropical forests has been limited, particularly in Africa. Hyperspectral data record canopy spectral information that is potentially related to forest biomass. To assess lidar ability to retrieve biomass in an African forest and the usefulness of including hyperspectral information, we modeled biomass using small footprint lidar metrics as well as airborne hyperspectral bands and derived vegetation indexes. Partial Least Square Regression (PLSR) was adopted to cope with multiple inputs and multicollinearity issues; the Variable of Importance in the Projection was calculated to evaluate importance of individual predictors for biomass. Our findings showed that the integration of hyperspectral bands ($R^2 = 0.70$) improved the model based on lidar alone ($R^2 = 0.64$), this encouraging result call for additional research to clarify the possible role of hyperspectral data in tropical regions. Replacing the hyperspectral bands with vegetation indexes resulted in a smaller improvement ($R^2 = 0.67$). Hyperspectral bands had limited predictive power ($R^2 = 0.36$) when used alone. This analysis proves the efficiency of using PLSR with small-footprint lidar and high resolution hyperspectral data in tropical forests for biomass estimation. Results also suggest that high quality ground truth data is crucial for lidar-based AGB estimates in tropical African forests, especially if airborne lidar is used as an intermediate step of upscaling field-measured AGB to a larger area.

1. Introduction

Remote sensing of forest aboveground biomass (AGB) has received increasing attention during the last decade due to its relevance to global carbon cycle modeling and to international programs aimed at reducing greenhouse gas emissions in tropical areas, such as the United Nations Reducing Emissions from Deforestation and Forest Degradation (REDD+). In particular, biomass mapping in tropical biomes is particularly important given the critical role of tropical forests in the global carbon cycle (Gibbs et al., 2007). Recent findings show that tropical forests store 21% more carbon than previously expected (Baccini et al., 2012). While the biomass of most temperate and boreal zones has been systematically inventoried at least once (Houghton et al., 2009), tropical regions suffer from operational limitations and consequent lack of data, which is especially marked in Africa (Baccini et al., 2008).

Airborne small-footprint Light Detection and Ranging (lidar) is considered the most accurate remote sensing technology for mapping biomass (Zolkos et al., 2013) and could be useful in filling this information gap. Discrete return (DRL) or full waveform (FWL) small-footprint lidar systems are now widespread and operated around the globe, enabling the collection of up to four returning energy pulses (as DRL) or all the returning energy (as FWL) from the forest vertical profile. The laser pulse returns are usually used

* Corresponding author at: CMCC – Centro Mediterraneo per i Cambiamenti Climatici, (Euro-Mediterranean Center for Climate Change), IAFENT Division, via Pacinotti 5, Viterbo 01100, Italy. Tel./fax: +39 06 72597710.
E-mail addresses: gaia.vagliolaurin@cmcc.it, laurin@disp.uniroma2.it (G. Vaglio Laurin).

0924-2716/$ - see front matter © 2014 International Society for Photogrammetry and Remote Sensing, Inc. (ISPRS) Published by Elsevier B.V. All rights reserved.
http://dx.doi.org/10.1016/j.isprsjprs.2014.01.001

to derive forest height metrics, which can then be related to field-observed AGB, with the latter obtained by means of field measures and allometric relationships. Due to the high operational costs, lidar-derived AGB estimates usually can only be obtained over limited areas. These local-scale or sub-national accurate estimates are crucial for REDD+ measuring, reporting, and verification (MRV), and for country level natural resources management and inventories (Næsset, 2007; Peterson et al., 2007). Local AGB maps are also the basis for the extension of estimates to larger areas using remote sensing approaches (Asner et al., 2010; De Sy et al., 2012). However, to date there has been little research into mapping of biomass in tropical forests using airborne small-footprint lidar. Zolkos et al. (2013) conducted a comprehensive review and identified eight studies carried out with this system in tropical forests, with none in continental Africa.

The uncertainties associated with the current knowledge of the African ecosystems' carbon balance are rather high. A review of the most recent estimates of the net long-term carbon balance of African ecosystems, based upon observations, indicated a sink of the order of 0.3 Pg Cyr^{-1} with a very high uncertainty and a variable source; up to now many questions remain open, and it is unclear whether Africa is a net carbon source or a sink to the atmosphere (Ciais et al., 2011). Because of highly variable CO_2 fluxes and insufficiently studied ecosystems and ecosystem–human–climate interactions, there is a need for continued and enhanced observations of carbon stocks, fluxes and atmospheric concentrations to enable more precise assessments of Africa's carbon cycle (Justice et al., 2001), and its sensitivity to natural and anthropogenic pressures and future climate. Of primary importance is the need for continent-wide carbon cycle observations that support both bottom-up and top-down methods of estimating carbon sources and sinks (Lewis et al., 2009). An African integrated carbon-observing system is needed, encompassing both: (i) regional inventories and monitoring of soil and vegetation carbon stocks by forest and agricultural research stations; (ii) remote sensing-based estimates of forest biomass C stock distribution, at different scales and using active and/or passive sensors combined with field observations. In view of the above considerations regarding the contributions of African forests in the global carbon cycle, it is clear how valuable it is to test biomass mapping by means of various sensors over different African forests.

Hyperspectral sensors, recording the reflectance of a large number of fine resolution spectral bands from visible to near infrared (NIR) or shortwave infrared (SWIR) range, are another frontier technology in remote sensing. Hyperspectral data can capture information regarding the biochemical composition of the upper canopy layer and have been used for forest type or species classification, estimation of biophysical and biochemical properties and health status (Asner and Martin, 2008; Koch, 2010; Goodenough et al., 2006). The ecosystem information recorded by hyperspectral data may relate to plant functional types – such as whether a species is light demanding – which could in turn affect wood density and thus biomass content (Baker et al., 2004; Chave et al., 2009). Hyperspectral data have been used to estimate grassland biomass directly (Cho et al., 2007; Psomas et al., 2011) and leaf canopy biomass (le Maire et al., 2008), while leaf area density, retrieved from fusion of hyperspectral and radar data, has been used in the estimation of forest AGB (Treuhaft et al., 2003). The few studies that have attempted to improve biomass estimates in boreal, temperate and tropical forests by combining hyperspectral imagery with lidar data have reported only modest or no improvement in model fit compared to the results from using lidar only (Anderson et al., 2008; Clark et al., 2011; Latifi et al., 2012; Swatantran et al., 2011). Despite these research efforts, the number of published studies on integrating lidar and hyperspectral data for biomass estimation is rather small. Further research is needed along this line, especially considering the opportunities from forthcoming hyperspectral missions, such as the Environmental Mapping and Analysis Program (EnMap), the PRecursore IperSpettrale of the application mission (PRISMA), the Medium Resolution Imaging Spectrometer (MERIS) and the Hyperspectral Infrared Imager (HyspIRI).

The main objectives of the present study are the following: (i) to test for the first time small footprint lidar-based AGB retrieval in a West African tropical moist forest, (ii) to examine whether the use of very high spatial resolution hyperspectral data in addition to lidar can improve the biomass estimates.

2. Materials and methods

2.1. Study area and ground truth data

The study area is within the Gola Rainforest National Park (GRNP) in Sierra Leone, at the westernmost end of the humid Upper Guinean Forest Belt, in West Africa (Fig. 1).

The forests of this region are largely lowland moist evergreen forest with some areas towards lowland dry evergreen and semi-deciduous forest types (Cole, 1993). Within GRNP Klop et al. (2008) identified moist evergreen, moist semi-deciduous, freshwater inland swamp forest, forest regrowth and secondary/disturbed forest. The GRNP area has been protected through conservation programs since 1989 but commercial logging, most intensively in the southern block, was carried out in 1963–1965 and 1975–1989. Recent land cover mapping (Vaglio Laurin et al., 2013) highlighted the importance of conserving this forest from anthropogenic pressure in the surrounding areas. The climate is moist tropical, with annual rainfall around 2500–3000 mm, a dry season from November to April coincident with leaf-off condition of some semi-deciduous tree species, and an altitude of 70–410 m.

Field data collection carried out in 2006–2007 in the GRNP established over 600 plots of 0.125 ha each across the whole park area, recording species information as well as structural and environmental forest parameters. In the plots, all trees with Diameter at Breast Height (DBH) > 30 cm were recorded, while trees with DBH included in the 10–30 cm range were measured in a 1/10 smaller subplot. Height measures were derived with a local DBH-height relationship and the AGB was obtained applying the Chave et al. (2005) general equation for moist tropical forest including DBH, height and wood density values. The data collection protocol and the allometric procedure are fully documented in Lindsell and Klop (2013). We selected all the plots surveyed by both lidar and hyperspectral sensors excluding some plots located less than 1 km from the park boundary where land cover changes were most likely to have occurred in the period between field and aerial data collection. We also excluded plots affected by cloud shadow in the hyperspectral data. We retained 70 ground truth plots, with an AGB range 0–586.9 Mg ha^{-1} (mean = 172.2 and standard deviation = 111.8 Mg ha^{-1}). These plots contained 136 species with DBH > 30 cm, and 86 occurring in the upper canopy layer.

2.2. Remote sensing data

The central and parts of the southern blocks of GRPN were surveyed by an airborne campaign in March 2012 over pre-defined flight lines covering part of the field, using a Pilatus PC-6 Porter aircraft equipped with lidar and hyperspectral sensors and a digital camera for aerial photographs.

The lidar sensor ALTM GEMINI (Optech Ltd.), characterized by a 1064 nm laser wavelength and able to record up to 4 range measurements, was operated between 650 and 850 m above ground level (AGL). The minimum laser density was set to 11 points/m^2. The

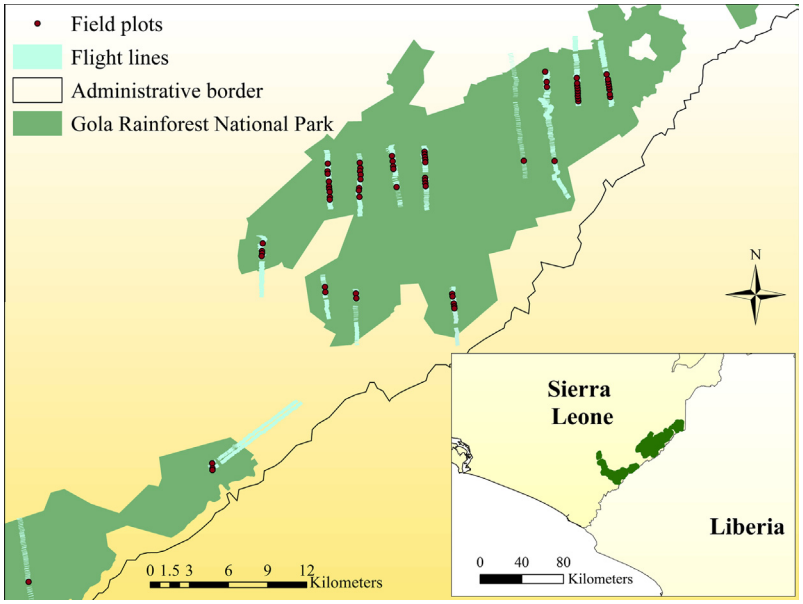

Fig. 1. The study area located along the border between Sierra Leone and Liberia, and included in the GRNP. The flight lines, realized during an airborne survey, cover part of the permanent field plots established in the Park.

lidar dataset was delivered as a point cloud of discrete returns, pre-processed in Terrascan (Terrasolid) software and adopted the ApplanixIN-Fusion™PPP Inertially-Aided Precise Point Positioning (IAPPP) to cope with the of absence of GPS base stations in the region. Positional error in x, y, z was always lower than 0.27 m for any axis. An additional check with points derived from the AUSPOS network of Geoscience Australia indicated a positional error lower than 0.2 m. The raw all-returns point cloud was processed using the Toolbox for Lidar Data Filtering and Forest Studies (TIFFS) (Chen, 2007) to derive a range of metrics for AGB estimation from each plot, including: mean height, quadratic mean height, skewness, kurtosis, height bins at 5 m intervals and 10% percentile heights. TIFFS used the ground returns identified by the data provider to generate a DTM (Digital Terrain Model) and calculated the relative height above terrain of each laser return by subtracting the corresponding DTM elevation from its original Z value. The lidar metrics were derived using the relative height of all laser points.

Hyperspectral data were acquired in 18 strips with an AISA Eagle sensor, with FOV equal to 39.7°, set to record 244 bands with 2.3 nm spectral resolution in the 400–970 nm range. The final spatial resolution was at 1 m after radiometric correction and orthorectification based on a lidar-derived Digital Elevation Model (DEM). A visual inspection of data from 30 randomly selected plots revealed a spatial mismatching between hyperspectral and lidar data within a range of 1–4 m.

Atmospheric correction of the hyperspectral images was performed using the Fast Line-of-Sight Atmospheric Analysis of Spectral Hypercubes (FLAASH) algorithm, which is based on a MODTRAN4 approach for path scattered radiance, absorption, and adjacency effects (Felde et al., 2003). Due to noise, all the bands outside the 450–900 nm range and four bands in the 759–766 nm range were removed, reducing the total number of bands to 186. Minimum Noise Fraction (MNF) transformation (Green et al., 1988) was used to further reduce noise in the dataset. For each image strip, 9–15 MNF components were selected by visual screening and used to compute the inverse MNF to transform back the bands in the original data space. Different strips have different noise levels and types: generally the useful information is included in the first 15 components, but this is a rule of thumb. Visual

Table 1
Description of remote sensing statistics used in biomass regression analyses.

Input	Description
Lidar height metrics	– Mean of all plot returns – Standard deviation – Quadratic mean – Skewness – Kurtosis – Proportion of points at height bins of 5 m intervals – 10% Percentiles from 10% to 100%
Hyperspectral bands	– 186 bands in the 450–900 nm interval, atmospherically corrected and noise minimized
Vegetation indices	– Normalized difference vegetation index (Sellers, 1985) – Simple ratio index (Sellers, 1985) – Atmospherically resistant vegetation index (Kaufman and Tanre, 1996) – Red edge normalized difference vegetation index (Sims and Gamon, 2002) – Vogelmann red edge index (Vogelmann et al., 1993) – Photochemical reflectance index (Gamon et al., 1992) – Red green ratio (Gamon and Surfus, 1999) – Anthocyanin reflectance index 2 (Gitelson et al., 2001)

screening allowed to identify the correct number of components to be used for analysis (Williams and Hunt, 2002; Underwood et al., 2003; Goodwin et al., 2005).

Eight vegetation indices (VIs) were calculated from the inverted MNF bands (Table 1): Normalized Difference Vegetation (NDVI) and Simple Ratio (SRI) (Sellers, 1985), Atmospherically Resistant Vegetation (ARVI) (Kaufman and Tanre, 1996), Red Edge Normalized Difference Vegetation (ReNDVI) (Sims and Gamon, 2002), Vogelmann Red Edge (VReI) (Vogelmann et al., 1993), Photochemical Reflectance (PRI) (Gamon et al., 1992), Red Green Ratio (GRI) (Gamon and Surfus, 1999), and Anthocyanin Reflectance 2 (AR2I) (Gitelson et al., 2001). These indices were chosen for representing information from different portions of the spectra of vegetation greenness, light use efficiency and leaf pigments and for being relatively insensitive to shadow. For each plot we averaged the VIs and the 186 hyperspectral bands after MNF inversion. Table 1 summarizes the lidar and hyperspectral inputs used in tests.

Aerial photographs were acquired simultaneously with lidar data using a Rollei H25 camera equipped with a Phase One Digital Back. Images were georeferenced and orthorectified using the lidar DEM. The orthophotos were acquired at 0.1 m spatial resolution, and used as reference for visual screening during data analysis (i.e. to visualize plot edge effects).

2.3. Retrieval models and tests

The large number of often correlated metrics from airborne lidar and hyperspectral data pose challenges in statistical modeling of biomass due to the problems of multicollinearity and "curse of dimensionality" (Adam and Mutanga, 2009; Dalponte et al., 2009). We used Partial Least Squares (PLSs) regression to deal with these issues. PLS regression is closely related to principal component regression (PCR), but differs in that it uses the information from the response variable in addition to the predictors for feature transformation (Geladi and Kowalski, 1986). PLS regression has been previously employed in spectral and chemical analysis of tropical forests (Asner and Martin, 2008), for AGB estimation (Lei et al., 2012; Goodenough et al., 2005), and as a method for dealing with large hyperspectral datasets (Peerbhay et al., 2013).

We modeled AGB from single and fused lidar and hyperspectral data, to understand the ability of our dataset to estimate AGB in an African rainforest, and assess the usefulness of these data integration. For hyperspectral data we tested both MNF-inverted bands and the derived VIs. The PLS regression results were compared with those obtained by a multiplicative power model (MPM), well suited to explain the usual power-law relationship occurring among biological parameters (Marquet et al., 2005). Inputs for both models were log transformed.

To develop the MPM, a forward stepwise regression of the log-transformed predictors and the AGB values was used to select the predictors; the initial model is then fitted using such predictors. Any of the selected predictors which were not significant from their p-value were removed ($p > 0.05$) and the model is refitted; the procedure was iterated until all predictors are statistically significant. For PLS regression, the transformed features were selected by minimizing the 10-fold cross-validation prediction error. A traditional method like MPM or other common statistical techniques is often used as a benchmark in literature for AGB estimation (Chen et al., 2012) or vegetation type discrimination (Vaglio Laurin et al., 2013). Comparison between MPM and PLS regression is useful to illustrate the accuracy improvement.

We calculated the Variable of Importance in the Projection (VIP) to evaluate importance of individual predictors for biomass estimation; predictors with VIP scores >1 are considered especially relevant for the mode l (Wold et al., 2001; Peerbhay et al., 2013).

3. Results

Based on lidar metrics alone, AGB was predicted with a coefficient of determination (R^2) equal to 0.64 and a RMSE of 67.8 Mg ha^{-1} using PLS; results obtained by MPM were less accurate ($R^2 = 0.57$). Hyperspectral bands had limited predictive power using PLS ($R^2 = 0.36$), and none with MPM. The VIs had very limited predictive power when entered into the models. Using PLS the addition of hyperspectral bands to lidar metrics increased the accuracy moderately ($R^2 = 0.70$, RMSE 61.7 Mg ha^{-1}), whilst replacing the hyperspectral bands with the VIs resulted in an even smaller improvement ($R^2 = 0.67$, RMSE 64.3 Mg ha^{-1}). No improvement of accuracy is obtained using MPM with combined lidar and hyperspectral dataset. In comparison to MPM, PLS produced improved accuracies in all models, except VIs alone. The AIC (Akaike's Information Criteria) was also calculated to compare different PLS models (Chen et al., 2007). In general, compared to the model with the lowest AIC value, the models with an AIC increase of 4–7 have considerable less support and the ones with an AIC increase of >10 have no support (Burnham and Anderson, 2002). Among our PLS models, the combination of lidar metrics and hyperspectral bands has the lowest AIC value of 597 and thus the best performance. The PLS model based on lidar metrics has an AIC value of 606, which corresponds to an increment of 9 and indicates that such a model is at least considerably worse than the model using both lidar metrics and hyperspectral bands. Table 2 illustrates the test results.

The scatterplots of the predicted vs. field observed AGB for different input combinations are presented in Fig. 3.

Among lidar metrics, the inputs obtaining VIP scores >1 included all percentiles (except the 10th and the 100th), some low range height bins, mean height and quadratic mean height. Highest scores were obtained, in descending order, by the 40th height percentiles, 30th height percentiles, mean height, 50th and 60th height percentiles. Among hyperspectral inputs, the higher scores were assigned to bands in the green, and red-edge region of the spectra, and in the near infrared region close to the end of the available spectra. When using the combined dataset, all lidar metrics received scores >1 and greater than the hyperspectral bands. Fig. 4 illustrates the most relevant input features selected by VIP procedure for the models based on single lidar and hyperspectral datasets.

Table 2
Test results obtained with different combinations of lidar metrics and hyperspectral features and through two different statistical models.

Inputs	Multiplicative Power Model (MPM)		Partial Least Square Regression (PLSR)		
	R^2	RMSE	R^2	RMSE	AIC
Lidar metrics	0.57	72.7	0.64	67.8	606
Hyperspectral bands	0.00	111.0	0.36	91.2	646
VIs	0.08	106.2	0.02	116.8	668
Lidar metrics + hyperspectral bands	0.57	72.7	0.70	61.7	597
Lidar metrics + VIs	0.57	72.7	0.67	64.3	601

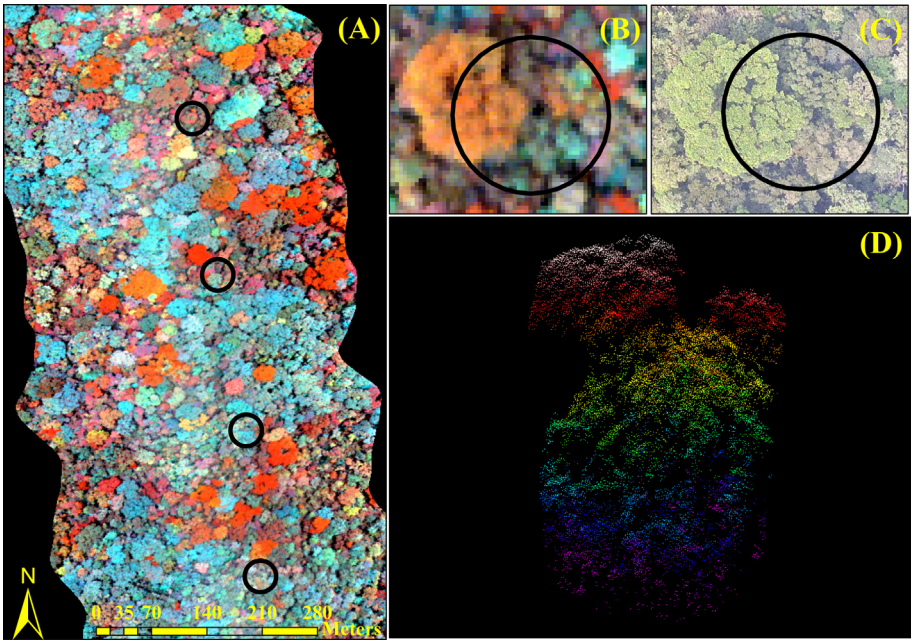

Fig. 2. In (A) and (B) false-color composite of hyperspectral data at 807.5 (R), 597.3 (G) and 467.3 (B) nm. In (A): strip of data where large crowns are visible. In (B): example of edge-effect for a specific plot. In (C): the same edge effect in (B) is visualized in the aerial photograph. Plot edges are represented as black circles. In (D): the same plot in (B) and (C) is visualized as a lidar point cloud.

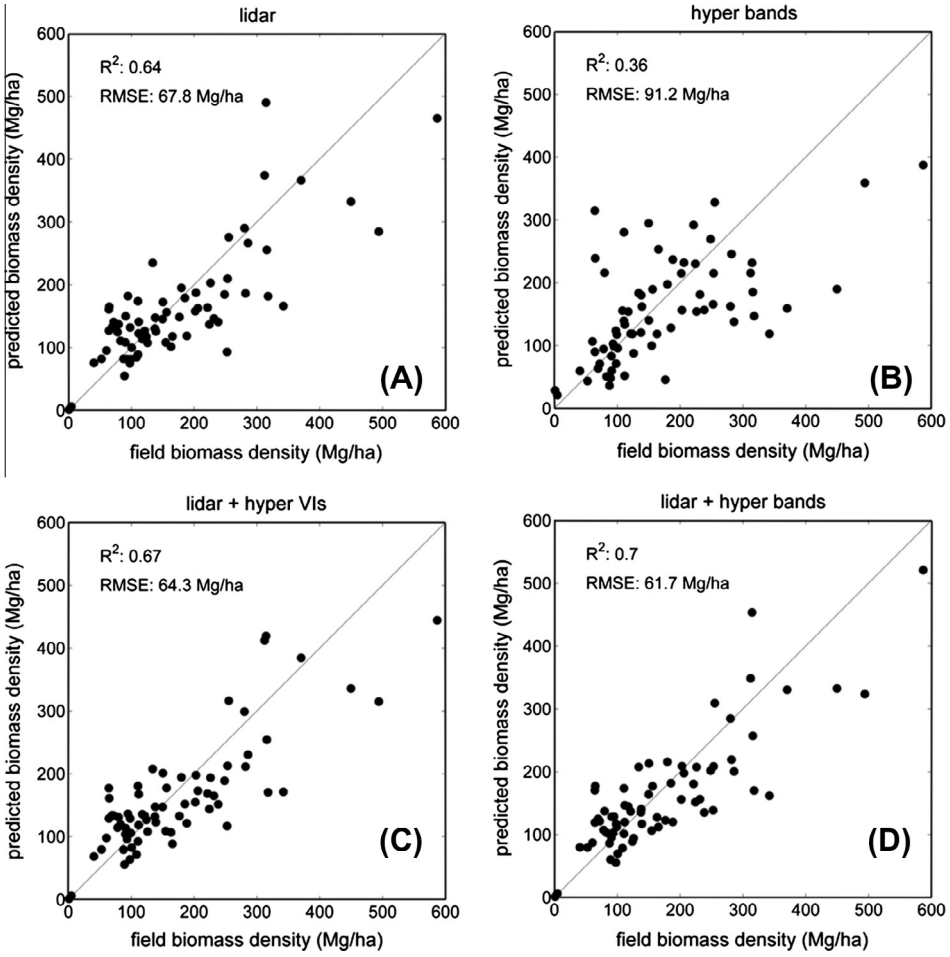

Fig. 3. Scatterplots of predicted vs. field observed AGB for the following inputs: (a) lidar metrics, (b) hyperspectral bands, (c) lidar metrics and VIs, (d) lidar metrics and hyperspectral bands.

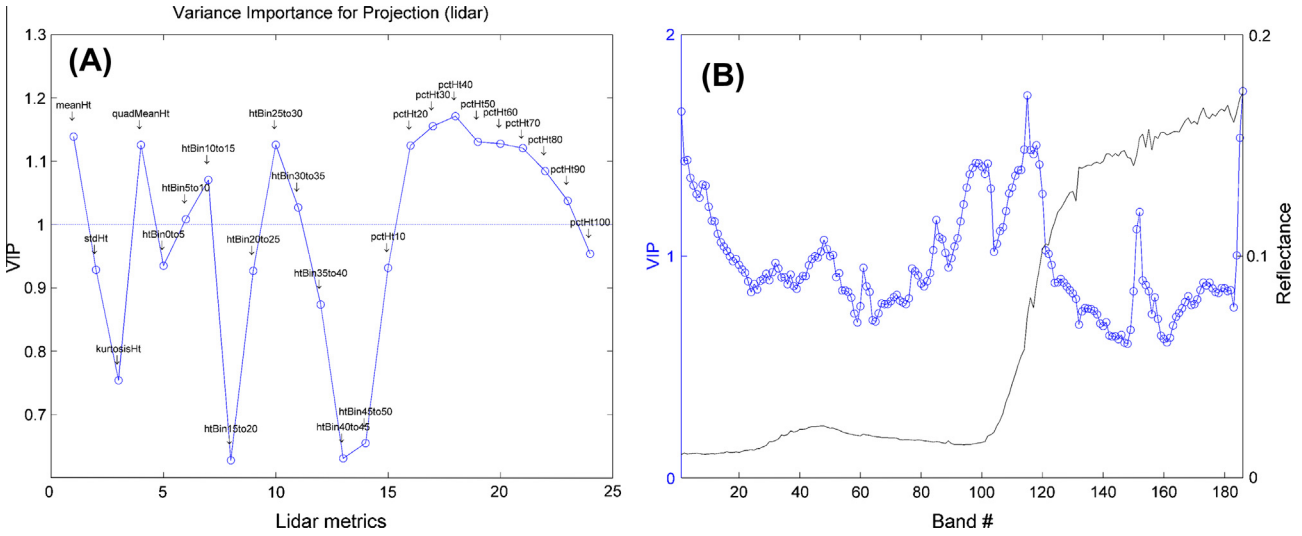

Fig. 4. VIP scores for individual lidar (a) and hyperspectral (b) datasets.

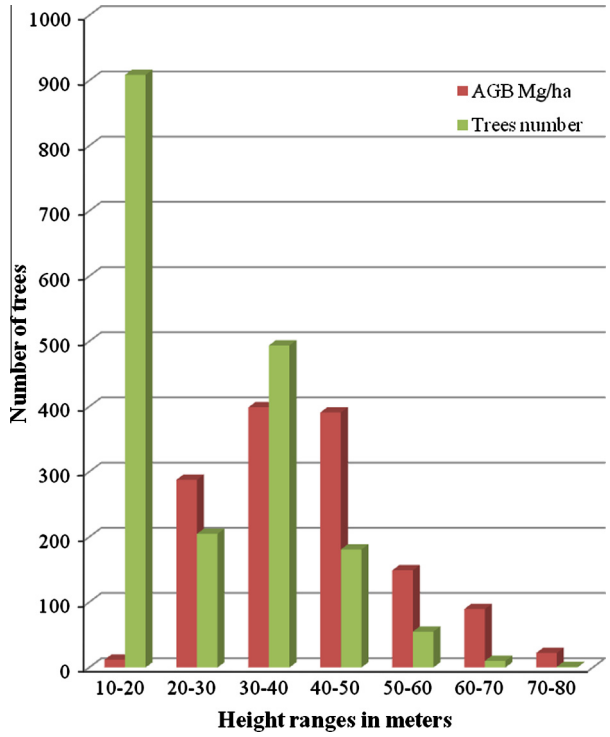

Fig. 5. AGB and number of trees in the 70 plots (total area = 87,500 m^2) according to different ranges of field-observed height.

To help understand the selection of relevant input feature by VIP for the lidar-based AGB model with respect to the forest structure, we graphically explored the distribution of trees and biomass in 7 classes of height, at 10 m intervals each (Fig. 5).

4. Discussion

4.1. Comparison to other studies of mapping tropical rainforest biomass

Our first aim was to test small footprint lidar for AGB estimation of an African tropical moist forest. The accuracy of our estimate is in within the range of those reported in other tropical studies that use small-footprint lidar (Asner et al., 2009, 2010; Asner et al., 2012b; Clark et al., 2011; d'Oliveira et al., 2012; Kennaway et al., 2008; Kronseder et al., 2012; Mascaro et al., 2011a). As far as we know, there are only two studies reporting usage of airborne lidar for mapping African tropical forests AGB (Asner et al., 2011, 2012a), both undertaken in Madagascar with a customized Optech 3100EA instrument (Carnegie Institution for Science, USA). The accuracy obtained in the current study is not far from that obtained in southeastern Madagascar (Asner et al., 2011), where 46 plots of 0.28 ha were used. After adopting improved allometric relationships to reflect regional variations in Madagascar, the authors reported a $R^2 = 0.68$ for their AGB estimate. However in the second study, Asner et al. (2012a) reported a higher result ($R^2 = 0.88$) for three combined sites, including humid and dry forests and shrubland on the island, for which improved allometric relations and differential correction of GPS measures were used. Per site results were not reported, and it is not clear if the dataset from the 2011 study was incorporated into the 2012 one, for which the authors reported a lower mean AGB.

We note that most tropical studies using small footprint lidar, which achieve high accuracy of the estimates, are based on plots more than double the area (0.28 ha) of our plots (Asner et al., 2009, 2010, 2011, 2012a,b; Mascaro et al., 2011b). Mascaro et al. (2011a,b)demonstrated in a tropical moist forest that lidar prediction error, which is strongly related to the edge effect, scales with plot area with a RMSE decreasing from 63.2 to 11.1 Mg C ha^{-1} when increasing the plot size from 0.04 ha to one hectare. Similar conclusions are given by Kohler and Huth (2010) for another tropical site. Furthermore, the edge effect – responsible for disagreement between remote sensing and field plot measures over which trees or parts of trees are inside the calibration plots – is more marked in small plots and in the presence of large tree crowns. In our study the plot size was less than the half of the size most commonly used in lidar calibration studies. Furthermore, since 25% of the measured trees had a DBH > 50 cm, the occurrence of edge effects was likely and indeed often observed, with plots frequently hosting very large crowns from neighboring mature trees (Fig. 2).

In contrast to studies which report that the higher lidar height percentiles explain most of the biomass variance (Patenaude et al., 2004; Skowronski et al., 2007), in our case the maximum VIP scores were assigned to the height percentiles included in the 30–60th range (Fig. 3a). This is an evidence of the multilayered structure of this mature forest, which possibly stores a large part of biomass in the subcanopy layer. This also indicates that the

biomass within a plot is not primarily driven by the tallest trees, which despite having the individually largest biomass values are nonetheless far less abundant than the mid-size trees (Fig. 5).

4.2. Sources of uncertainties

The relatively low accuracy (the best R^2 was 0.70) we obtained in this study could be associated with different sources of uncertainty including: field measurement errors, plot locations errors, and errors introduced by the allometric model. These errors, together with error caused by geometrical and radiometric correction of remotely sensed data, are well known sources of uncertainty in remote sensing analysis (Lu et al., 2012).

In our datasets, there was a 5–6 years time lag between field and remote sensing data acquisitions. Even if the growth of a mature forest in a 5-year period is limited, this temporal mismatch can still cause errors in estimates due to natural mortality and regeneration. We exclude plots located close to GRNP border to limit the probability of abrupt forest changes, such as those resulting from illegal clearance or tree harvesting. It is known that forest biomass grows at different rates according to its successional stages (Hudak et al., 2012) and even in mature forests areas of regeneration are present due to natural tree mortality.

In our study site, plot locations were measured using a recreational Garmin GPS. Obtaining accurate GPS measures can be difficult in tall and dense forests; as well as in regions which lack base stations that allow for differential correction (Dominy and Duncan, 2001), as was the case in our study area. Chen et al. (2012) reported that the use of plot locations measured by uncorrected GPS decreased the R^2 of the AGB estimates by 0.10–0.13 and increased the RMSE by about 21–31% in the mixed conifer forests of California.

Biomass mapping in Africa suffers from a major lack of regional specific allometric equations. According to studies conducted in the region (Henry et al., 2010; Djomo et al., 2010) the best available option is to use the Chave et al. (2005) general equations. Nevertheless, these equations were obtained without including African tree samples and the issue of their validity in Africa is still debated due to limited data for comparative research. The generic allometric equation that we used could be a major uncertainty. For example Henry et al. (2010) estimated a difference of approximately 40% in AGB values using site-specific vs. generalized allometric equations in West Africa.

The control of uncertainty sources, such as those here mentioned, can be a bigger challenge in African forests than in other areas. Most of the African countries lack the technical and financial capacities for field measures extensive collection, and very limited infrastructure to support scientific research is available (Avitabile et al. (2011), Baccini et al., 2008). The establishment of a field network to collect quality ground truth for calibration of remote sensing data, and the development of regional allometric equations, are two major issues to which international programs should direct their support.

4.3. Lidar and hyperspectral data fusion

The addition of hyperspectral features to lidar resulted in an increase of R^2 values from 0.64 to 0.70 (Table 2), which is a slightly greater improvement than has been found in previous studies (Chen, 2013). In northern biomes, Anderson et al. (2008) and Swatantran et al. (2011) obtained respectively modest and insignificant improvement using the Laser Vegetation Imaging Sensor (LVIS) and Airborne Visible/Infrared Imaging Spectrometer (AVIRIS) fused datasets. Their results are difficult to compare with ours, due to the coarser resolution of those sensors and the difference in forests types. Swatantran et al. (2011) suggested that the predictive power of hyperspectral could be higher when lidar relationships with biomass are weaker, as observed by Anderson et al. (2008) and Roth (2009). This hypothesis is in part confirmed by our results, in which the lidar-AGB relationship is not as high as elsewhere and an increase in accuracy was brought by inclusion of hyperspectral data. Latifi et al. (2012) used very high spatial resolution sensors, namely a full waveform lidar and HyMap. They also reported minimal improvement in AGB estimates from fused datasets, using PCR. The PLS regression used in this study is preferable to PCR, which might account for the difference. The only AGB estimation for a tropical area, carried out using a FLI MAP lidar and the hyperspectral HYDICE sensor, reported no improvement by the addition of hyperspectral VIs and spectral mixture fractions to lidar metrics (Clark et al., 2011), similar to the very small improvement we observed using our VIs. The increase in accuracy observed with hyperspectral original bands in our study can be explained by the ability of PLS to exploit information from the whole spectrum. The use of VIs, based on a limited subset of spectral bands, possibly excludes important bands for biomass estimation.

Our visual assessment indicates that there is ~1–4 m co-registration mismatching between hyperspectral and lidar data, which complicates our evaluation of hyperspectral data for biomass estimation. Given the geometric accuracy of airborne small-footprint lidar usually being sub-meter horizontally, it would be ideal if the georeferencing accuracy of hyperspectral is at the sub-meter level as well, to maximize the use of information from both sensors. This requires precise orthorectification of hyperspectral imagery, preferably based on a Digital Surface Model (DSM) instead of a Digital Terrain Model (DTM) because of the relief displacement caused by trees. This georeferencing accuracy issue has to be taken into account for prospective use of hyperspectral data in AGB estimation, for which the mismatch with reference or other data can be higher.

Latifi et al. (2012) and Papes et al. (2010) found that the most useful spectral ranges for estimating vegetation biomass are green and the NIR plateau, while Zhang et al. (2009) assumed that the greenness indices might have a positive potential toward predicting AGB. The VIP scores in our study confirmed that the green and NIR portion of the spectra were useful for biomass estimation, but higher scores were obtained for bands in the red-edge (Fig. 2b). It is widely recognized that the red-edge position relates to the health status of photosynthetic material in the vegetation (Horler et al., 1983) but it is unclear how this correlates with biomass variation, which calls for more future research along this line. The AISA Eagle sensor used in this study has a wavelength range of ~400–900 nm, which can be a limitation considering that other studies in literature have proved the significance of longer wavelengths (SWIR) for vegetation (Brown et al., 2000; Psomas et al., 2011), in particular Gong et al. (2003) proved that SWIR and NIR bands are most important for LAI estimation.

AGB-lidar modeling can be improved by stratifying the vegetation types using optical imagery or ancillary data (Clark et al., 2011; Garcia et al., 2010). Chen et al. (2012) illustrated the positive effect of integrating vegetation type maps derived by aerial photography in Sierra Nevada, using a mixed effects model. In temperate or boreal forests, dominated by few species and where vegetation type maps are often available, this approach can be feasible. However, it is less clear how hyperspectral-based stratification could be carried out in a tropical forest as our site, having very high diversity of tree species, often without marked dominance, and where detailed information on vegetation type is usually not present. The high number of tree species and thus variations in tree morphology, beside variations in spectral responses, can be a reason for explaining the fact that biomass estimation cannot be based on hyperspectral data alone. As a matter of fact literature shows that it is more useful in low-biomass

scenarios like grasslands where some studies show that up to 61% of variation can be explained by VIs from hyperspectral data only (Clevers et al., 2007).

5. Conclusions

REDD+ advocates better documentation of performances of remote sensing data across ranges of biomes, vegetation cover, topography/land forms, seasons, and land use patterns that occur across developing countries (Holmgren, 2008). Recently, the 17th Conference of the Parties (COPs) to the United Nation Convention on Climate Change (UNFCCC) adopted the commitment that national REDD+ monitoring and reporting systems shall be based on a combination of field measurements and remote sensing data. Even if clear standards have not yet been established, the Global Climate Observing System (GCOS, 2011) suggested some accuracy levels, driven by the need to quantify carbon stocks to initialize and test the carbon cycle and for national reporting, which are: <20% error for biomass values over 50 Mg/ha, and 10 Mg/ha for biomass values < 50 t/ha. Houghton et al. (2009) also suggested a maximum of 18% AGB uncertainty. In the case of mature tropical forests, with mean AGB often over 200 Mg/ha, this translates to an error below 40 Mg/ha which is often difficult to achieve even with very advanced tools such as lidar systems. For large area AGB estimation in tropical environments, direct AGB retrieval based on radar sensors, which have full mapping and all weather capabilities, could thus be a cost-effective alternative to lidar sampling followed by further upscaling, especially if new dedicated missions will be launched, such as the European Space Agency Biomass.

Our research evidences that high quality ground truth data, especially in terms of geolocation accuracy and larger plot size, is needed when planning lidar-based AGB estimates in tropical African forests, Our results suggest that the quality of ground truth data can be even more important if airborne lidar is used as an intermediate step of upscaling field-measured AGB to a larger area or region, a procedure with associated additional uncertainty.

The methodology here presented includes an advanced retrieval algorithm (PLS), significant preprocessing with innovative techniques applied to hyperspectral data (MNF) and a method for testing different features from data fusion. Such a straightforward workflow can provide a robust method for evaluating the importance of spectral contributions and lidar metrics.

The findings related to hyperspectral and lidar data fusion presented in this research are encouraging, but call for additional research. The possible role of hyperspectral data in direct AGB estimation or stratification has to be clarified in different environments, and new VIs that can incorporate relevant biomass information could be developed. As vegetation characteristics strongly influence the sensors ability to retrieve information, additional research in various ecosystems is needed to be able to generalize conclusions about the usefulness of joint sensors use. Overall this study contributes to enlarge research on lidar and hyperspectral fused datasets applicability and provide interesting insight which could orient future sensors development and missions.

Acknowledgements

We acknowledge the ERC grant Africa GHG #247349 and the Cambridge Conservation Initiative for providing additional support to the investigation. Field plot data were collected by staff of the Gola Forest Programme, a collaboration between the Government of Sierra Leone's Forestry Department, the Conservation Society of Sierra Leone and The RSPB, with funding from the UK's Darwin Initiative. We are grateful for the assistance of the staff of the Gola Rainforest National Park, in particular the Protected Area Manager Mr. Alosine Fofana, the Gola Forest Project Leader Guy Marris as well as Dr. Annika Hillers and Dr. Aida Cuni Sanchez of the RSPB for their support in organizing the lidar flight. We are also very grateful to "Wildlife" Mansary of the Forestry Department for his assistance with permissions for the flight.

References

Adam, E., Mutanga, O., 2009. Spectral discrimination of papyrus vegetation (*Cyperus papyrus L.*) in swamp wetlands using field spectrometry. ISPRS J. Photogramm. Remote Sens. 64 (6), 612–620.

Anderson, J.E., Plourde, L.C., Martin, M.E., Braswell, B.H., Smith, M.L., Dubayah, R.O., Hofton, M.A., Blair, J.B., 2008. Integrating waveform LiDAR with hyperspectral imagery for inventory of a northern temperate forest. Remote Sens. Environ. 112, 1856–1870.

Asner, G.P., Martin, R.E., 2008. Spectral and chemical analysis of tropical forests: scaling from leaf to canopy levels. Remote Sens. Environ. 112, 3958–3970.

Asner, G., Flint, Hughes.R., Varga, T., Knapp, D., Kennedy-Bowdoin, T., 2009. Environmental and biotic controls over aboveground biomass throughout a tropical rain forest. Ecosystems 12 (2), 261–278.

Asner, G.P., Powell, G.V.N., Mascaro, J., Knapp, D.E., Clark, J.K., Jacobson, J., Kennedy Bowdoin, T., Balaji, A., Paez-Acosta, G., Victoria, E., Secada, L., Valqui, M., Hughes, R.F., 2010. High-resolution forest carbon stocks and emissions in the Amazon. Proc. Nat. Acad. Sci. USA 107 (38), 16738–16742.

Asner, G.P., Mascaro, J., Muller-Landau, H.C., Vieilledent, G., Vaudry, R., Rasamoelina, M., Hall, J.S., van Breugel, M., 2011. A universal airborne LiDAR approach for tropical forest carbon mapping. Oecologia 168, 1147–1160.

Asner, G., Clark, J., Mascaro, J., Vaudry, R., Chadwick, K.D., Vieilledent, G., Rasamoelina, M., Balaji, A., Kennedy-Bowdoin, T., Maatoug, L., Colgan, M., Knapp, D., 2012a. Human and environmental controls over aboveground carbon storage in Madagascar. Carbon Balance Manage. 7, 2.

Asner, G.P., Clark, J.K., Mascaro, J., Galindo Garcia, G.A., Chadwick, K.D., Navarrete Encinales, D.A., Paez-Acosta, G., Cabrera Montenegro, E., Kennedy-Bowdoin, T., Duque, A., Balaji, A., von Hildebrand, P., Maatoug, L., Phillips Bernal, J.F., Knapp, D.E., Garcia Davila, M.C., Jacobson, J., Ordonez, M.F., 2012b. High-resolution mapping of forest carbon stocks in the Colombian Amazon. Biogeosci. Discuss. 9 (3), 2445–2479.

Avitabile, V., Herold, M., Henry, M., Schmullius, C., 2011. Mapping biomass with remote sensing: a comparison of methods for the case study of Uganda. Carbon Balance Manage. 6, 7.

Baccini, A., Laporte, N., Goetz, S.J., Sun, M., Dong, H., 2008. A first map of Tropical Africa's above-ground biomass derived from satellite imagery. Environ. Res. Lett. 045011.

Baccini, A., Goetz, S.J., Walker, W.S., Laporte, N.T., Sun, M., Sulla-Menashe, D., Hackler, J., Beck, P.S.A., Dubayah, R., Friedl, M.A., Samanta, S., Houghton, R.A., 2012. Estimated carbon dioxide emissions from tropical deforestation improved by carbon-density maps. Nature Climate Change 2, 182–185.

Baker, T.R., Phillips, O.L., Malhi, Y., Almeida, S., Arroyo, L., Di Fiore, A., Erwin, T., Higuchi, N., Killeen, T.J., Laurance, S.G., Laurance, W.F., Lewis, S.L., Lloyd, J., Monteagudo, A., Neill, D.A., Patino, S., Pitman, N.C.A., Silva, J.N.M., Vasquez Martinez, R., 2004. Variation in wood density determines spatial patterns in Amazonian forest biomass. Glob. Change Biol. 10, 545–562.

Brown, L., Chen, J.M., Leblanc, S.G., Cihlar, J., 2000. A shortwave infrared modification to the simple ratio for LAI retrieval in boreal forests: an image and model analysis. Remote Sens. Environ. 71, 16–25.

Burnham, K.P., Anderson, D.R., 2002. Model Selection and Multimodel Inference: A Practical Information-Theoretic Approach, second ed. Springer-Verlag Press, New York.

Chave, J., Andalo, C., Brown, S., Cairns, M.A., Chambers, J.Q., Eamus, D., Fölster, H., Fromard, F., Higuchi, N., Kira, T., Lescure, J.P., Nelson, B.W., Ogawa, H., Puig, H., Riéra, B., Yamakura, T., 2005. Tree allometry and improved estimation of carbon stocks and balance in tropical forests. Oecologia 145 (1), 78–99.

Chave, J., Coomes, D., Jansen, S., Lewis, S.L., Swenson, N.G., Zanne, A.E., 2009. Towards a worldwide wood economics spectrum. Ecol. Lett. 12 (4), 351–366.

Chen, Q., 2007. Airborne lidar data processing and information extraction. Photogramm. Eng. Remote Sens. 73 (2), 109–112.

Chen, Q., Gong, P., Baldocchi, D.D., Xie, G., 2007. Filtering airborne laser scanning data with morphological methods. Photogramm. Eng. Remote Sens. 73 (2), 175–185.

Chen, Q., Vaglio, Laurin.G., Battles, J., Saah, D., 2012. Integration of airborne lidar and vegetation types derived from aerial photography for mapping aboveground live biomass. Remote Sens. Environ. 121, 108–117.

Chen, Q., 2013. Lidar remote sensing of vegetation biomass. In: Weng, Q., Wang, G. (Eds.), Remote Sensing of Natural Resources, CRC Press: Taylor & Francis, Group, pp. 399–420.

Cho, M.A., Skidmorea, A., Corsi, F., van Wieren, S.E., Sobhana, I., 2007. Estimation of green grass/herb biomass from airborne hyperspectral imagery using spectral indices and partial least squares regression. Int. J. Appl. Earth Obs. Geoinf. 9 (4), 414–424.

Ciais, P., Bombelli, A., Williams, M., Piao, S.L., Chave, J., Ryan, C.M., Henry, M., Brender, P., Valentini, R., 2011. The carbon balance of Africa: synthesis of recent research studies. Philos. Trans. Roy. Soc. A 369, 2038–2057.

Clark, M.L., Roberts, D.A., Ewel, J.J., Clark, D.B., 2011. Estimation of tropical rain forest aboveground biomass with small-footprint LiDAR and hyperspectral sensors. Remote Sens. Environ. 115, 2931–2942.
Clevers, J.G.P.W., van der Heijden, G.W.A.M., Verzakov, S., Schaepman, M.E., 2007. Estimating grassland biomass using SVM band shaving of hyperspectral data. Photogramm. Eng. Remote Sens. 73 (10), 1141–1148.
Cole, N.H.A., 1993. Floristic association in the Gola rain forests: a proposed biosphere reserve. J. Pure Appl. Sci. 2, 35–50.
Dalponte, M., Bruzzone, L., Vescovo, L., Gianelle, D., 2009. The role of spectral resolution and classifier complexity in the analysis of hyperspectral images of forest areas. Remote Sens. Environ. 133 (11), 2345–2355.
De Sy, V., Herold, M., Achard, F., Asner, G.P., Held, A., Kellndorfer, J., Verbesselt, J., 2012. Synergies of multiple remote sensing data sources for REDD+ monitoring. Curr. Opin. Environ. Sustain. 4, 696–706.
d'Oliveira, M.V.N., Reutebuch, S.E., McGaughey, R.J., Andersen, H.E., 2012. Estimating forest biomass and identifying low-intensity logging areas using airborne scanning lidar in Antimary State Forest, Acre State, Western Brazilian Amazon. Remote Sens. Environ. 124, 479–491.
Dominy, N.J., Duncan, B., 2001. GPS and GIS methods in an African rain forest: applications to tropical ecology and conservation. Conserv. Ecol. 5 (2), 6.
Djomo, A.N., Ibrahima, A., Saborowski, J., Gravenhorst, G., 2010. Allometric equations for biomass estimations in Cameroon and pan moist tropical equations including biomass data from Africa. For. Ecol. Manage. 260, 1873–1885.
Felde, G.W., Anderson, G.P., Cooley, T.W., Matthew, M.W., Adler-Golden, S.M., Berk, A., Lee, J., 2003. Analysis of Hyperion data with the FLAASH atmospheric correction algorithm. In: Proceedings of the International Geoscience and Remote Sensing Symposium, Toulouse, France, (IGARSS'03), pp. 90–92.
Gamon, J.A., Penuelas, J., Field, C.B., 1992. A narrow-waveband spectral index that tracks diurnal changes in photosynthetic efficiency. Remote Sens. Environ. 41, 35–44.
Gamon, J.A., Surfus, J.S., 1999. Assessing leaf pigment content and activity with a reflectometer. New Phytol. 143, 105–117.
Garcıa, M., Riano, D., Chuvieco, E., Danson, M., 2010. Estimating biomass carbon stocks for a Mediterranean forest in central Spain using LiDAR height and intensity data. Remote Sens. Environ. 114, 816–830.
GCOS, 2011. Report 154 – Systematic observation requirements for satellite-based products for climate supplemental details to the satellite-based component of the implementation plan for the global observing system for climate in support of the UNFCCC – 2011 Update, December 2011.
Geladi, P., Kowalski, B.R., 1986. Partial least-squares regression: a tutorial. Anal. Chim. Acta 185, 1–17.
Gibbs, H.K., Brown, S., Niles, J.O., Foley, J.A., 2007. Monitoring and estimating tropical forest carbon stocks: making REDD a reality. Environ. Res. Lett. 2, 045023.
Gitelson, A.A., Merzlyak, M.N., Chivkunova, O.B., 2001. Optical properties and nondestructive estimation of anthocyanin content in plant leaves. Photochem. Photobiol. 71, 38–45.
Gong, P., Pu, R., Biging, G.S., Larrie, M.R., 2003. Estimation of forest leaf area index using vegetation indices derived from hyperion hyperspectral data. IEEE Trans. Geosci. Remote Sens. 41 (6), 1355–1362.
Goodenough, D.G., Li, J.Y., Dyk, A., 2006. Combining hyperspectral remote sensing and physical modeling for applications in land ecosystems. In: IEEE International Geoscience And Remote Sensing Symposium (IGARSS 2006), Denver, Colorado, vol. 1–8.
Goodenough, D.G., Han, T., Dyk, A., Gour, J., Li, J.Y., 2005. Mapping forest biomass with AVIRIS and evaluating SNR impact on biomass prediction. Natural Resources Canada, internal report, (presented at NASA JPL AVIRIS Workshop, May, Pasadena, California).
Goodwin, N., Coops, N.C., Stone, C., 2005. Assessing plantation canopy condition from airborne imagery using spectral mixture analysis and fractional abundances. Int. J. Appl. Earth Obs. Geoinf. 7 (1), 11–28.
Green, A.A., Berman, M., Switzer, P., Craig, M.D., 1988. A transformation for ordering multispectral data in terms of image quality with implications for noise removal. IEEE Trans. Geosci. Remote Sens. 26 (1), 65–74.
Henry, M., Besnard, A., Asante, W.A., Eshun, J., Adu-Bredu, S., Valentini, R., Bernoux, M., Saint-André, L., 2010. Wood density, phytomass variations within and among trees, and allometric equations in a tropical rainforest of Africa. For. Ecol. Manage. 260, 1375–1388.
Hudak, A.T., Strand, E.K., Vierling, L.A., Byrne, J.C., Eitel, J., Martinuzzi, S., Falkowski, M.J., 2012. Quantifying aboveground forest carbon pools and fluxes from repeat LiDAR surveys. Remote Sens. Environ. 123, 25–40.
Holmgren, P., 2008. Role of satellite remote sensing in REDD. United Nations REDD Programme, MRV Working Paper series, 13 October 2008.
Horler, D.N.H., Dockray, M., Barber, J., 1983. The red edge of plant leaf reflectance. Int. J. Remote Sens. 4 (2), 273–278.
Houghton, R.A., Hall, F.G., Goetz, S.J., 2009. The importance of biomass in the global carbon cycle. J. Geophys. Res. – Biogeosci. 114 (G2).
Justice, C., Wilkie, D., Zhang, Q., Brunner, J., Donoghue, C., 2001. Central African forests, carbon and climate change. Climate Res. 17 (2), 229–246.
Kaufman, Y.J., Tanre, D., 1996. Strategy for direct and indirect methods for correcting the aerosol effect on remote sensing: from AVHRR to EOS-MODIS. Remote Sens. Environ. 55, 65–79.
Kennaway, T.A., Helmer, E.H., Lefsky, M.A., Brandeis, T.A., Sherrill, K.R., 2008. Mapping land cover and estimating forest structure using satellite imagery and coarse resolution lidar in the Virgin Islands. J. Appl. Remote Sens. 2 (1), 1–27.
Klop, E., Lindsell J., Siaka A., 2008. Biodiversity of Gola Forest, Sierra Leone. Royal Society for the Protection of Birds, Conservation Society of Sierra Leone, Government of Sierra Leone.
Koch, B., 2010. Status and future of laser scanning, synthetic aperture radar and hyperspectral remote sensing data for forest biomass assessment. ISPRS J. Photogramm. Remote Sens. 65 (6), 581–590.
Kohler, P., Huth, A., 2010. Towards ground-truthing of spaceborne estimates of above-ground life biomass and leaf area index in tropical rain forests. Biogeosciences 7, 2531–2543.
Kronseder, K., Ballhorn, U., Böhm, V., Siegert, F., 2012. Above ground biomass estimation across forest types at different degradation levels in Central Kalimantan using LiDAR data. Int. J. Appl. Earth Obs. Geoinf. 18, 37–48.
Lei, C., Ju, C., Cai, T., Jing, X., Wei, X., Di, X., 2012. Estimating canopy closure density and above-ground tree biomass using partial least square methods in Chinese boreal forests. J. Forest. Res. 23 (2), 191–196.
le Maire, G., François, C., Soudani, K., Berveiller, D., Pontailler, J.Y., Bréda, N., Genet, H., Davi, H., Dufrêne, E., 2008. Calibration and validation of hyperspectral indices for the estimation of broadleaved forest leaf chlorophyll content, leaf mass per area, leaf area index and leaf canopy biomass. Remote Sens. Environ. 112, 3846–3864.
Latifi, H., Faßnacht, F., Koch, B., 2012. Forest structure modeling with combined airborne hyperspectral and LiDAR data. Remote Sens. Environ. 121, 10–25.
Lewis et al., 2009. Increasing carbon storage in intact African tropical forests. Nature 457, 1003–1006.
Lindsell, J.A., Klop, E., 2013. Spatial and temporal variation of carbon stocks in a lowland tropical forest in West Africa. For. Ecol. Manage. 289, 10–17.
Lu, D., Chen, Q., Wang, G., Moran, E., Batistella, M., Zhang, M., Vaglio Laurin, G., Saah, D., 2012. Aboveground forest biomass estimation with Landsat and LiDAR data and uncertainty analysis of the estimates. Int. J. Forest. Res. Article ID 436537.
Marquet, P.A., Quiñones, R.A., Abades, S., Labra, F., Tognelli, M., Arim, M., Rivadeneira, M., 2005. Scaling and power-laws in ecological systems. J. Exp. Biol. 208, 1749–1769.
Mascaro, J., Asner, G.P., Muller-Landau, H.C., van Breugel, M., Hall, J., Dahlin, K., 2011a. Controls over aboveground forest carbon density on Barro Colorado Island, Panama. Biogeosciences Discussions 7 (6), 8817–8852.
Mascaro, J., Detto, M., Gregory, P.A., Muller-Landau, H.C., 2011b. Evaluating uncertainty in mapping forest carbon with airborne LiDAR. Remote Sens. Environ. 115, 3770–3774.
Næsset, E., 2007. Airborne laser scanning as a method in operational forest inventory: status of accuracy assessments accomplished in Scandinavia. Scand. J. For. Res. 22 (5), 433–442.
Patenaude, G., Hill, R.A., Milne, R., Gaveau, D.L.A., Briggs, B.B.J., Dawson, T.P., 2004. Quantifying forest above ground carbon content using LiDAR remote sensing. Remote Sens. Environ. 93 (3), 368–380.
Papes, M., Tupayachi, R., Martinez, P., Peterson, A.T., Powel, G.V.N., 2010. Using hyperspectral satellite imagery for regional inventories: a test with tropical emergent trees in the Amazon Basin. J. Veg. Sci. 21, 342–354.
Peerbhay, K.Y., Mutanga, O., Ismail, R., 2013. Commercial tree species discrimination using airborne AISA Eagle hyperspectral imagery and partial least squares discriminant analysis (PLS-DA) in KwaZulu–Natal, South Africa. ISPRS J. Photogramm. Remote Sens. 79, 19–28.
Peterson, B., Dubayah, R., Hyde, P., Hofton, M., Blair, J.B., Fites-Kaufman, J., 2007. Use of LIDAR for forest inventory and forest management application. In: McRoberts, Ronald E.; Reams, Gregory A., Van Deusen, Paul C., McWilliams, William H. (Eds.), Proceedings of the Seventh Annual Forest Inventory and Analysis Symposium; October 3–6, 2005; Portland, ME. Gen. Tech. Rep. WO-77. Washington, DC: US Department of Agriculture, Forest Service: 193–202.
Psomas, A., Kneubuhler, M., Huber, S., Itten, K., Zimmermann, N.E., 2011. Hyperspectral remote sensing for estimating aboveground biomass and for exploring species richness patterns of grassland habitats. Int. J. Remote Sens. 32 (24), 9007–9031.
Roth, K.L., 2009. A combined lidar and hyperspectral remote sensing analysis for mapping forest biomass. Unpublished master thesis. University of California, Santa Barbara, Dept of Geography.
Sellers, P.J., 1985. Canopy reflectance, photosynthesis, and transpiration. Int. J. Remote Sens. 6, 1335–1372.
Sims, D.A., Gamon, J.A., 2002. Relationships between leaf pigment content and spectral reflectance across a wide range of species, leaf structures and developmental stages. Remote Sens. Environ. 81, 337–354.
Skowronski, N., Clark, K., Nelson, R., Hom, J., Patterson, M., 2007. Remotely sensed measurements of forest structure and fuel loads in the pinelands of New Jersey. Remote Sens. Environ. 108 (2), 123–129.
Swatantran, A., Dubayah, R., Roberts, D., Hofton, M., Blair, J.B., 2011. Mapping biomass and stressin the Sierra Nevada using lidar and hyperspectral data fusion. Remote Sens. Environ. 115, 2917–2930.
Treuhaft, R.N., Asner, G.P., Law, B.E., 2003. Structure-based forest biomass from fusion of radar and hyperspectral observations. Geophys. Res. Lett. 30 (9), 1472–1479.
Underwood, E., Ustin, S., DiPietro, D., 2003. Mapping nonnative plants using hyperspectral imagery. Remote Sens. Environ. 86 (2), 150–161.
Vaglio Laurin, G., Liesenberg, V., Chen, Q., Guerriero, L., Del Frate, F., Bartolini, A., Coomes, D., Wilebore, B., Lindsell, J., Valentini, R., 2013. Optical and SAR sensor synergies for forest and land cover mapping in a tropical site in West Africa. Int. J. Appl. Earth Obs. Geoinf. 21, 7–16.
Vogelmann, J.E., Rock, B.N., Moss, D.M., 1993. Red edge spectral measurements from sugar maple leaves. Int. J. Remote Sens. 14, 1563–1575.

Williams, A.P., Hunt, E.R., 2002. Estimation of leafy spurge cover from hyperspectral imagery using mixture tuned matched filtering. Remote Sens. Environ. 82 (2–3), 446–456.

Wold, S., Sjostrom, M., Eriksson, L., 2001. PLS-regression: a basic tool of chemometrics. Chemometr. Intell. Lab. Syst. 58 (2), 109–130.

Zhang, H., Hu, H., Yao, X., Zheng, K., 2009. Estimation of above-ground biomass using HJ-1 hyperspectral images in Hangzhou Bay, China. In: International Conference on Information Engineering and Computer Science, 2009. ICIECS 2009.

Zolkos, S.G., Goetz, S.J., Dubayah, R., 2013. A meta-analysis of terrestrial aboveground biomass estimation using lidar remote sensing. Remote Sens. Environ. 128, 289–298.